ICEYE support within GAMMA Software

Urs Wegmüller, Christophe Magnard, Gamma Remote Sensing AG

Version 15-Aug-2023 (updated)

1. INTRODUCTION

In this document the support provided in the GAMMA Software for the processing of data of the ICEYE X-band SAR satellites is summarized. The first ICEYE X-band SAR satellites X1 and X2 were launched in 2018. Further satellites followed in 2019 and 2021, including X6 in a 1-day repeat orbit that is better suited for repeat-pass interferometry. For details on the mission see the ICEYE web-site at www.iceye.com.

In the following the importing of the ICEYE data is described, followed by an assessment of some available data sets, in particular concerning interferometric techniques.

2. IMPORTING ICEYE DATA

2.1. Importing SLC data

ICEYE SLC data are provided as a HDF5 files, that can be read / imported using the program ***par_ICEYE_SLC***:

par_ICEYE_SLC ../Mojave_orig/ICEYE_X6_SLC_SM_48793_20210321T203536.h5 20210321.slc.par 20210321.slc 0

As input the HDF5 file is indicated. The program generates the SLC binary data file, in SCOMPLEX or FCOMPLEX format, and the related SLC parameter file. The SLC can be visualized using

disSLC 20210321.slc 19563 1 2000 1. .35 0

and the spectrum can be checked using

dismph_fft 20210321.slc 19563 1 2000 1. .35 128 3 0

We check the quality of the orbit state vectors using *ORB_filt_spline.py*.

/bin/cp 20210321.slc.par 20210321.slc.par.orig

ORB_filt_spline.py 20210321.slc.par.orig 20210321.slc.par --png png_dir --degree 5

The quality looks good (except for a tiny quantification ripple at < 0.001 m level. No outliers or cm level noise are identified. The statistics show a 0.4 mm standard deviation of the unfiltered state vector positions from the filtered solution. The generated png file that shows the positional deviations is shown in Figure 1.

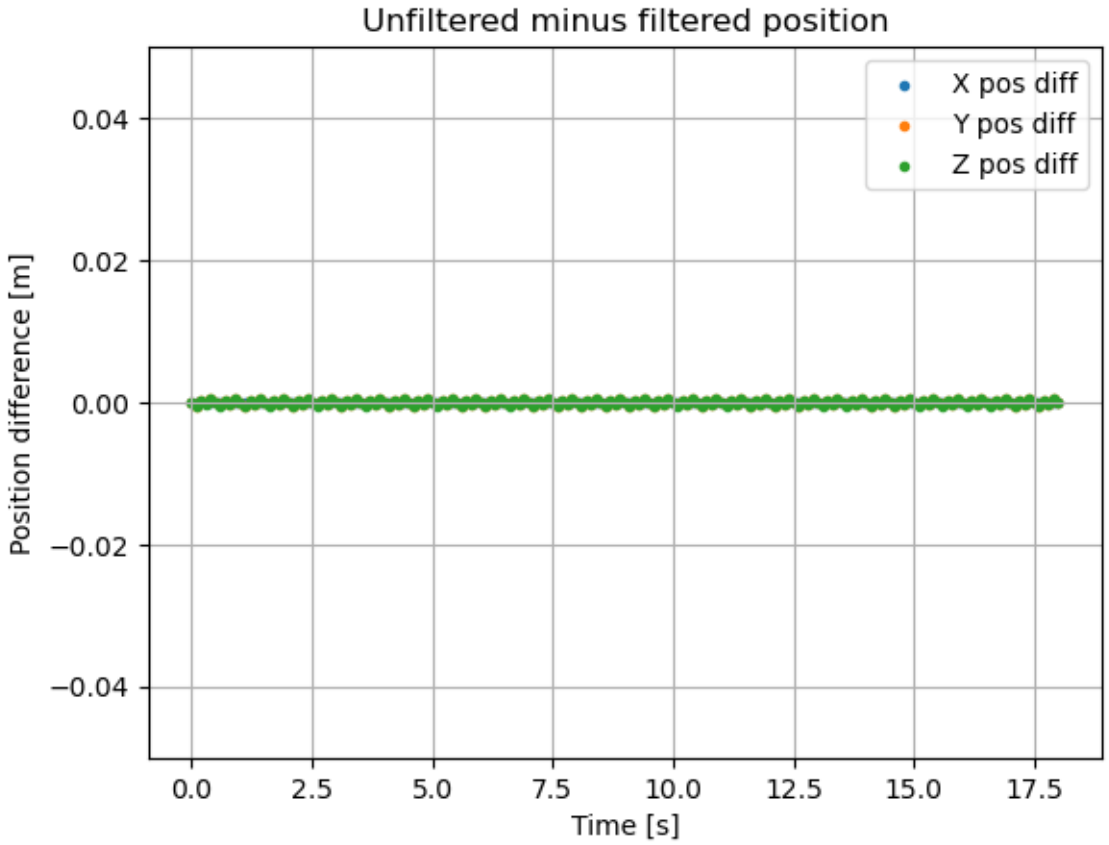


Figure 1 State vector deviations from the filtered solution. There is a tiny periodic ripple, most likely a quantification effect, of the order < 0.001 m. There are no outliers identified.

Using the SLC we generate a backscatter image in slant range geometry. Considering the sampling of the SLC

range_pixel_spacing: 0.9225119 m
azimuth_pixel_spacing: 1.4276166 m
incidence_angle: 27.9956 degrees

we select

multi_look 20210321.slc 20210321.slc.par 20210321.mli 20210321.mli.par 4 5

ras_dB 20210321.mli 4890 1 - 1 1 -10 10 gray.cm 20210321.mli.bmp 0 0

The resulting backscatter image is shown in Figure 2.

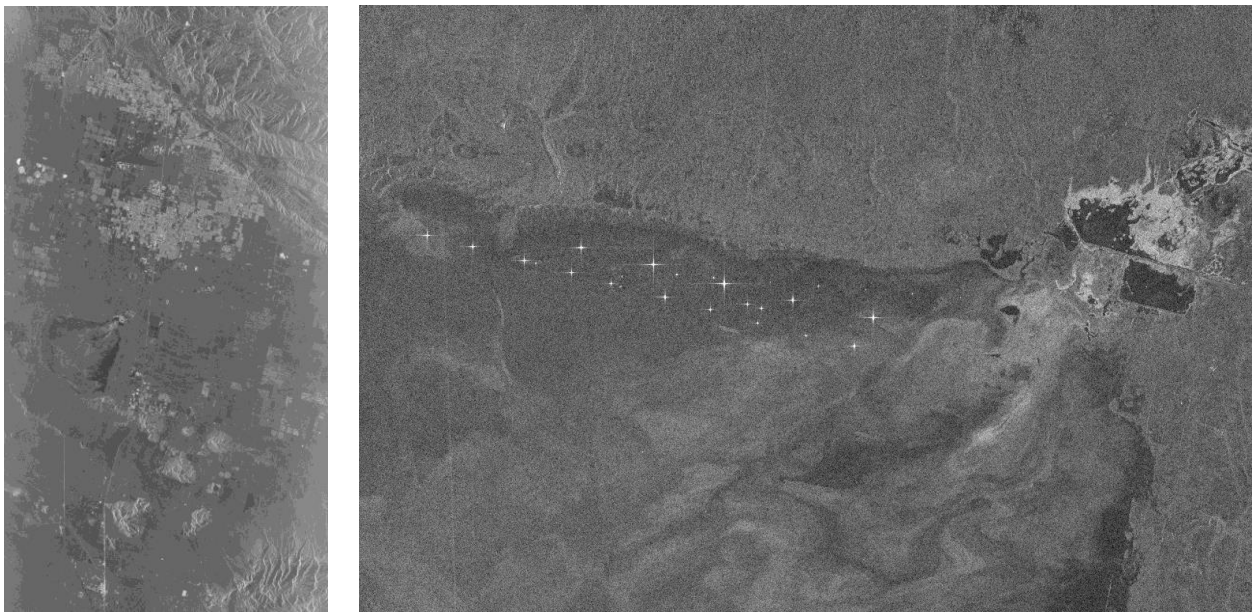


Figure 2 An overview on the scene (left) and a section of it that includes a Corner Reflector range (right) of ICEYE X6 stripmap mode data (4 x 5 look MLI in slant range geometry).

2.2. Importing detected data in ground range geometry

So-called detected GRD (ground-range) products can be imported using *par_ICEYE_GRD*. In the reading step the geometry is transferred from the ground-range geometry to (the better defined) slant-range geometry. Geocoding, multi-looking etc is then done in slant range geometry or after geocoding the backscatter images to a map geometry.

3. ASSESSMENT OF SOME CHARACTERISTICS OF ICEYE SLC

3.1. Radiometric calibration and estimation of NESZ

The corner reflectors present in the Mojave scene could be used to determine calibration factors. Information on the corner reflector dimensions and orientation is available at https://uavsar.jpl.nasa.gov/cgi-bin/calibration.pl. We did not determine our own calibration factors but we are using what is provided by ICEYE. In the *multi_look* step we did not further scale the values.

Using dark areas (radar shadow and smooth water surfaces) we estimated a Noise Equivalent Sigma Zero (NESZ) value. In mid-range this value is around -16 dB to -17 dB. In the near and far range higher values up to about -12 dB were observed. Considering that targets with lower than -10 dB backscatter are quite frequent such high NESZ values result in low backscatter contrast and the coherence of interferograms is significantly reduced.

3.2. Point target characteristics

Considering the corner reflectors present in the scene (Figure 2) we determined the following point target characteristics using the program *ptarg_SLC*:

slant range resolution (3dB):	0.93 m
azimuth resolution (3dB):	2.4 m
peak_side_lobe_ratio:	< -14.7 dB

3.3. Geocoding

We generated a multi-look intensity image using 4 range and 5 azimuth looks and conducted a geocoding sequence, using the 1-arc-second Copernicus DEM. As part of the geocoding sequence a refinement is determined based the offset between a simulate backscatter image (calculated based on the orbit data and the DEM) and the actual SAR backscatter.

The refinement statistics indicate for the offset estimates a very small standard deviation of below 0.2 multi-look pixel in both slant range azimuth. For the data acquired in 2021 the determined range and azimuth offsets are also very small (< 20m).

The small refinement values in the geocoding and also in the co-registration of other SLCs to the selected reference SLC indicate a high orbit state vector quality.

3.4. Offset tracking

In the frame of the EUROSTARS RAMON project we had access to a large stack of ICEYE-X6 stack acquired over Disko Island. For the interferometric analysis of the data we co-registered all the SLC to a common reference SLC. The co-registration was done based on the orbit data and considering the Copernicus DEM heights of the area. In addition, a refinement of the co-registration (with a constant range and azimuth offset) was done. The co-registered SLC were then used to generate interferograms.

Starting from the co-registered SLCs determined positional offset fields. Positional offsets are of interested to map meter scale displacements such as glacier motion. Furthermore, positional offsets in the azimuth direction are of interest in the context of ionospheric path delay effects. And positional offsets may allow to identify imperfect SAR data processing.

We generated offsets fields using an intensity matching technique on the co-registered SLC stack. This was done for different time intervals. Reliable offset maps with an almost complete spatial coverage were obtained mainly for short time intervals. Figures 3 and 4 show examples of range and azimuth offset fields.

The range offsets (Figure 3) observed correspond at large scale to a slight linear trend. Small errors in the orbit data, meta data or in the processing done may have caused these errors. Applying in the co-registration not just a constant but also linear terms allows to avoid these offsets. The small remaining range offsets relate then to the topography.

The azimuth offsets (Figure 4) observed show smaller scale variation in the range direction and distinct jumps in the azimuth direction. We interpret this as a clear indication of some “processing issues”. The along-track variation seems continuous but relatively small scale. The cross-track variation is distinct with clear jumps in the azimuth offset. We are not sure what the origin for the observed azimuth offsets is. The along-track variation might relate to imperfect interpolation of the orbit data (e.g. the velocity data). The distinct jumps in the azimuth direction may related to the use of different processing parameters for different range blocks.

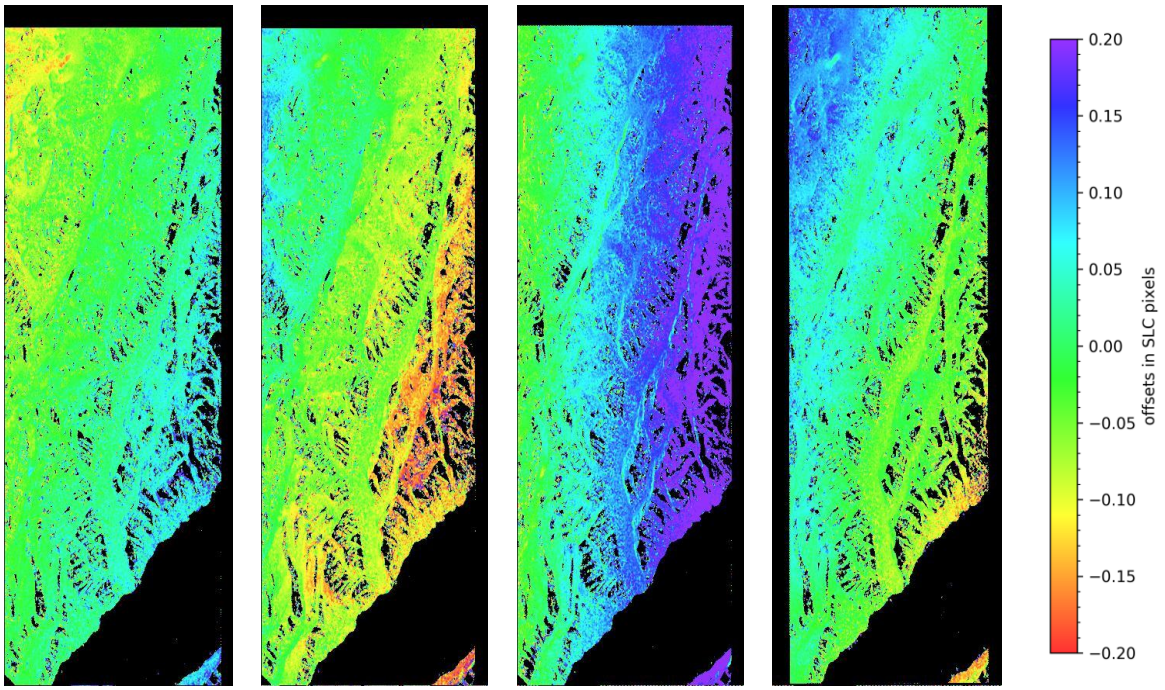
To find out the origin of the anomaly we did a direct co-registration of the pair with bi-linear offset polynomials and found a very similar effect in the azimuth offsets determined for these co-registered SLCs. So we conclude that the issue is most likely not caused by “an error in the state vector data” but seems to be “in the SLC data” (related to the raw data processing).

In the interferometric time series analysis the scene acquired on 20211226 was not considered (poor co-registration statistics, low coherence). The offset field relative to the scene acquired one day earlier, on 20211225, indicates what the problem is (Figure 5). Range offsets > 3 pixel and azimuth offsets up to more than 7 pixel are observed.

To check if the anomaly is “in the SLC data” or “in the orbit state vectors” we did a direct co-registration of the pair with bi-linear offset polynomials. We did not find a similar effect in the azimuth offsets determined just based on the SLC data sets, so we conclude that the issue is most likely caused by “an error in the state vector data”. This was also confirmed using the orbit state vector filtering program (Figure 6).

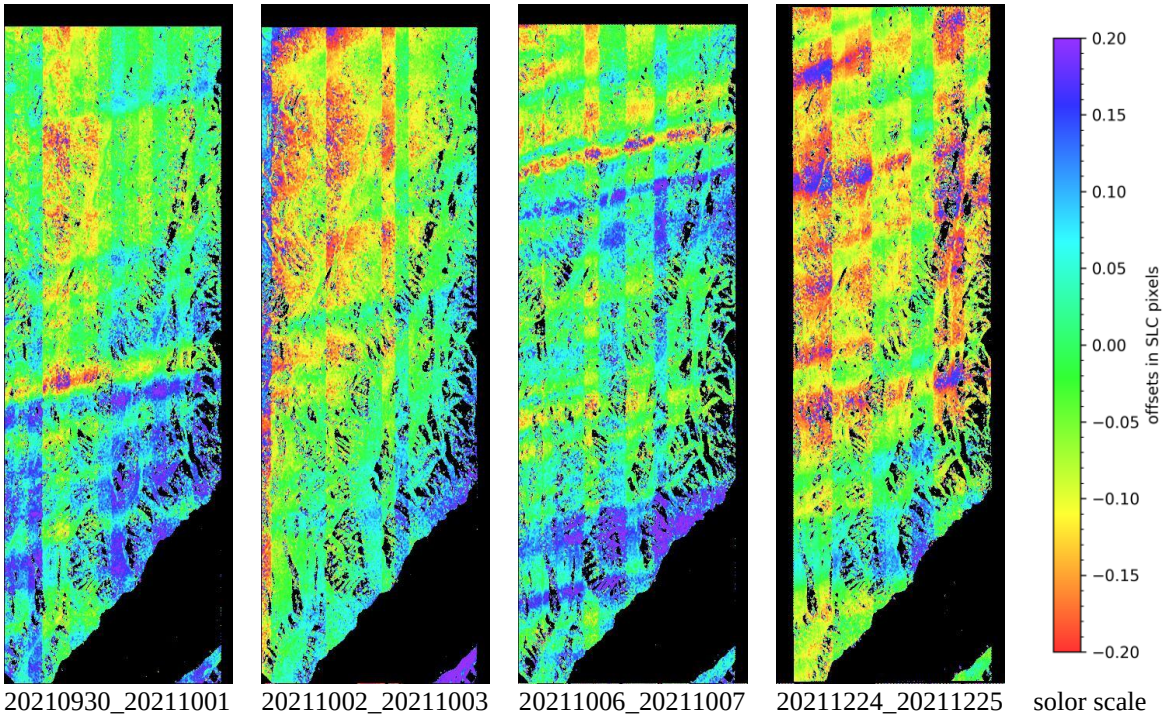
Using offset tracking we identified two issus with ICEYE data over Disko Island:

1) The SLC seem to have azimuth positional offsets up to about 0.2 SLC pixels. The azimuth positional offsets show distinct jumps in the range direction and variation without jumps in the azimuth direction. Offsets at this level should not significantly affect the interferometric phase or coherence.
2) For the acquisition of 20211226 a few orbit state vector positions deviate from a smooth track by several meters. To identify and mitigate this we recommend therefore to always check the state vector quality using *ORB_filt_spline.py*.



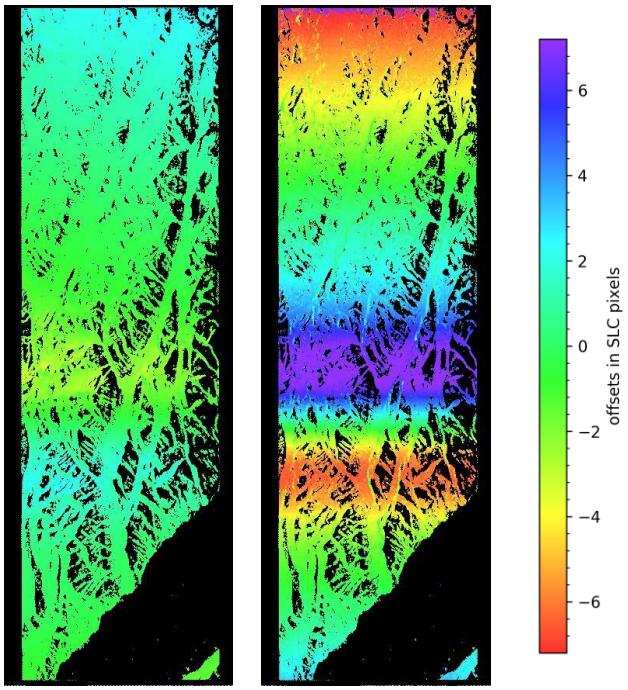
20210930_20211001 20211002_20211003 20211006_20211007 20211224_20211225 solor scale

Figure 3 Range offsets determined for selected pairs of the co-registered SLC stack over Disko Island, shown in slant range geometry. Notice the fine color scale. At large spatial scale the observed offsets correspond to a slight overall trend. Such a trend could be corrected by considering also linear terms in the co-registration refinement.



20210930_20211001 20211002_20211003 20211006_20211007 20211224_20211225 solor scale

Figure 4 Azimuth offsets determined for selected pairs of the co-registered SLC stack over Disko Island, shown in slant range geometry. Notice the fine color scale. The observed offsets show a significant variation in azimuth direction and distinct jumps in the range direction. The offsets are < 0.2 pixel, consequently the coherence of interferograms is not much reduced.



range offset field azimuth offsests color scale

Figure 5 Range and azimuth offsets determined for the pair 20211225_20211226 of the co-registered SLC stack over Disko Island, shown in slant range geometry. The color scale is between -7.2 and +7.2 pixel. The observed offsets show a significant variation in azimuth direction.

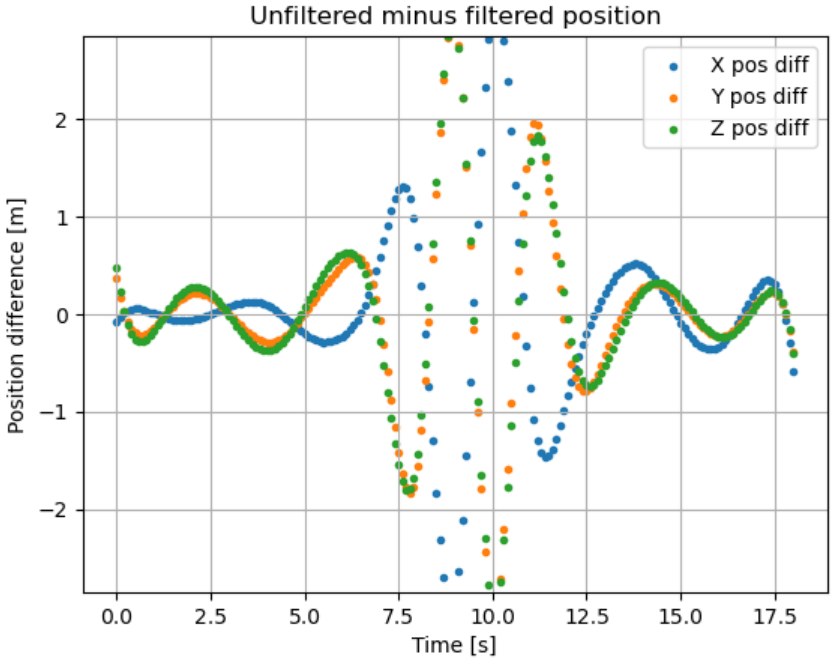


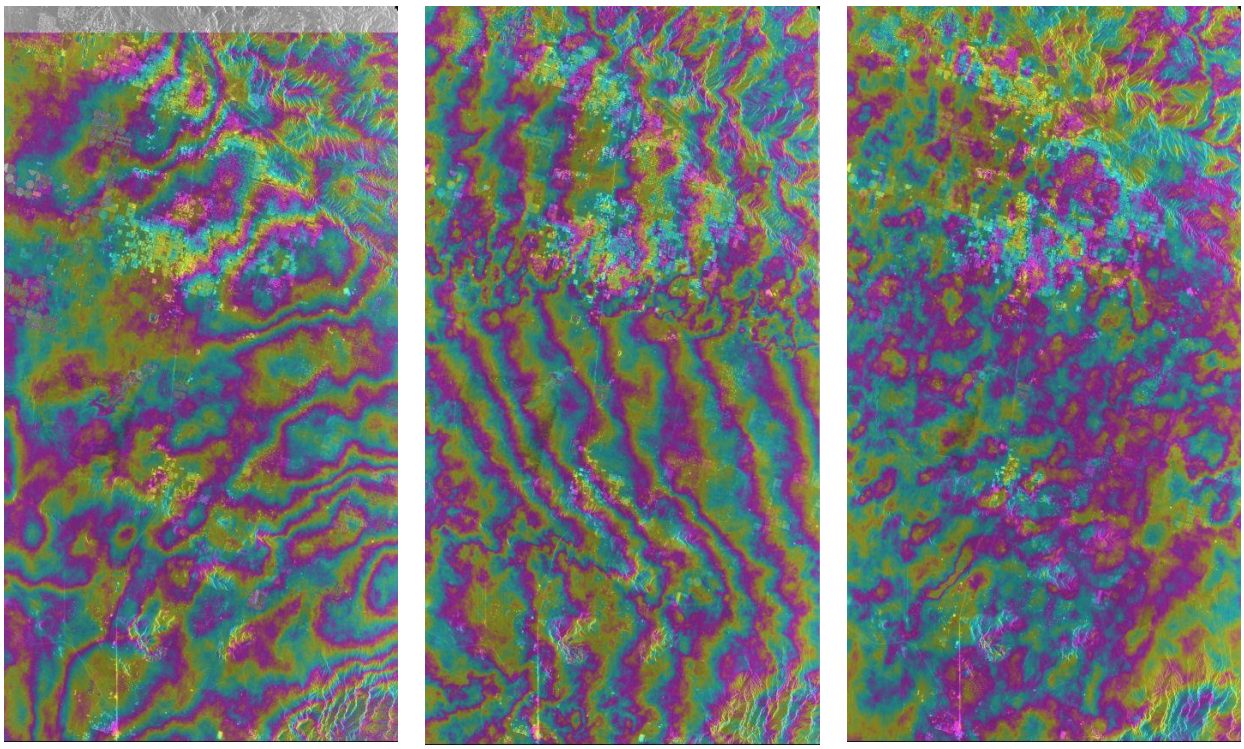
Figure 6 State vector deviations from the filtered solution for the acquisition on 26-Dec-2021. There is clear meter scale deviation of the filtered solution from the unfiltered solution, indicating outliers.

4. ICEYE DIFFERENTIAL SAR INTERFEROMETRY

4.1. Processing sequence used

Our early ICEYE InSAR tests with X2 and X4 data were affected by very large spatial baselines. The orbit control was not very strict and so suited baselines below 1km were very rare. Then with X6, operated in a 1-day repeat cycle, this changed. The orbital drift between subsequent acquisitions was often around 200m. So pairs with short spatial and temporal baselines became available. Thanks stacks of more than 50 scenes we could assess not only differential interferometry but also time series analysis approaches.

For differential interferometry we first selected and geocoded the reference scene. Then each SLC was co-registered to the reference scene using *SLC_coreg*. Then the normal sequence (*create_offset*, *phase_sim_orb*, *SLC_diff_intf*) was used. Examples of differential interferograms are shown in Figure 7.



20210215_20210409, dt=53d, $B_\perp$= 61m | 20210308_20210309, dt=1d, $B_\perp$=-358m | 20210415_20210416, dt=1d, $B_\perp$=-111m

Figure 7 Examples of differential interferograms over Mojave, USA.

As stated above the NESZ in the near and far range is quite high (around -12 dB). As a consequence of the high NESZ the interferograms are also expected to be more noisy in these regions. The coherence factor related to the backscattering coefficient and the NESZ is calculated as

$$\gamma_{noise} = \frac{\sigma_0}{\sigma_0 + NESZ}$$

So for $\sigma_0 = 1 * NESZ$ the resulting coherence is 0.5, for $\sigma_0 = 2 * NESZ$ 0.67, and for $\sigma_0 = 10 * NESZ$ 0.91.

To assess this effect we calculated and averaged the coherence over a large number of interferograms with short spatial and temporal baselines. As expected generally lower coherence levels are observed in the near and far range because of the high *NESZ* (Figure 8).

For InSAR the lower coherence means more phase noise. Spatial multi-looking (and/or filtering) can be used to reduce the phase noise for a given coherence.

Besides the large scale effect related to the NESZ spatial variation of the coherence related to landcover is observed. Stable areas (rocks, buildings, gravel) show the highest values, slightly vegetated areas reduced levels, and dense vegetation and water surfaces very low values.



Figure 8 Average coherence over all ICEYE differential interferograms with time intervals ≤ 3 days and baselines < 200m (linear scaling between 0.1 and 0.8).

Interferometric time series analysis

The stack of 2D differential interferograms over Mojave was then also used to assess the potential for time series analysis. For this we did not work with single pixel phase (corresponding to point-like scatterers) but using multi-look interferogram phases. This choice was made to possibly get a better spatial coverage for the relatively flat arid areas.

The satellite orbit was drifting first in one direction and then towards the end in the other direction. To get a better independence of baselines and time intervals we selected a stack with generally short spatial baselines, but including "longer" time intervals (see Figure 9).

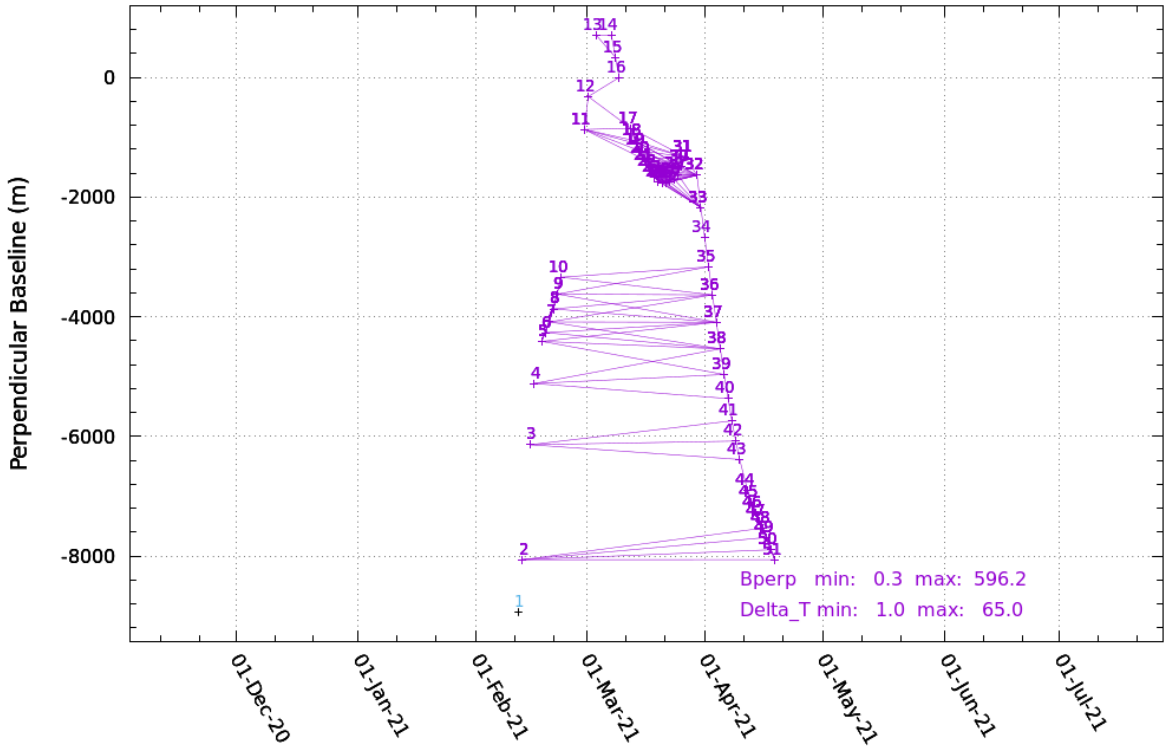


Figure 9 Time-baseline plots for the short baseline and short time interval pairs used in the average coherence estimation (top) and for the stack used in the time-series analysis (bottom).

Based on the stack we determined height corrections, atmospheric phases and the displacement phase time series. The estimation error for the average displacement rate is high because of the short total time period covered by the data. mm/year deformation could not reliably be determined. But in a salt lake area displacement at cm scale between the first and the last date could be observed.

The quality of the estimated DEM heights, on the other hand, is high as it is based on many interferograms, also including pairs with longer spatial baselines.

Figure 10 shows the estimated heights, and for comparison the Copernicus 1arc second DEM heights for a small relatively flat section. Overall the ICEYE based heights correspond closely to the Copernicus 1arc second DEM heights. Fine structures are more clearly visible in the ICEYE based DEM. Furthermore, the salt lake area shows less variation for the salt lake area which can be assumed flat. So thanks to the high spatial resolution and the significant data stack available the Copernicus DEM heights could be improved.

The coherence and the phase standard deviation calculate for the redundant InSAR stack (another measure for the phase noise) are shown in Figure 10. We observe a high correspondence of the two different "phase noise" measures. Areas with low backscatter show a low coherence and high phase noise. At least partly this may be related to the high signal noise in these areas.

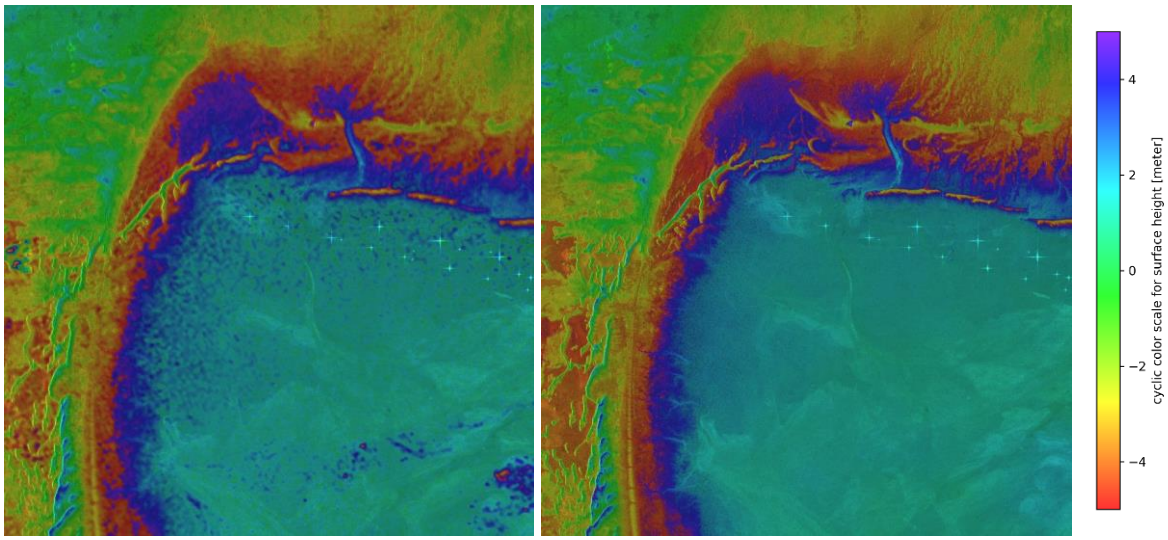


Figure 9 Oversampled 1-arc-second Copernicus DEM height (left) and ICEYE based updated DEM for an 5.6km x 5.6 km area (section 1) including parts of a salt lake area with corner reflectors. A fine cyclic color scale was used to make difference between the two height maps better visible.

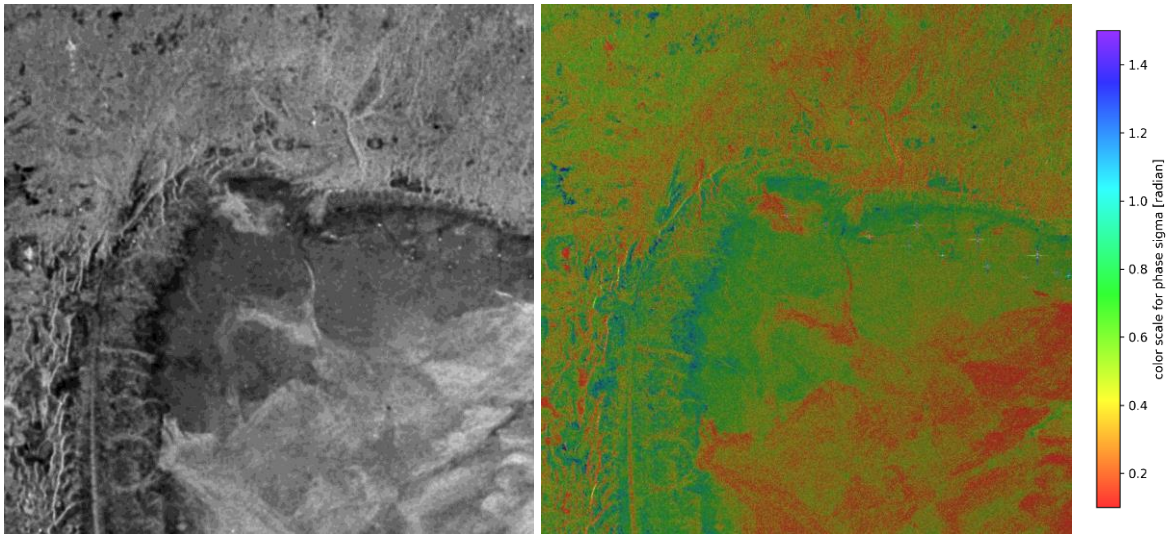


Figure 10 Average coherence of pairs with baselines up to 200m and time intervals up to 3 days (left, linear gray scale) and phase standard deviation calculate for the redundant InSAR stack (right, using color scale shown to the right).

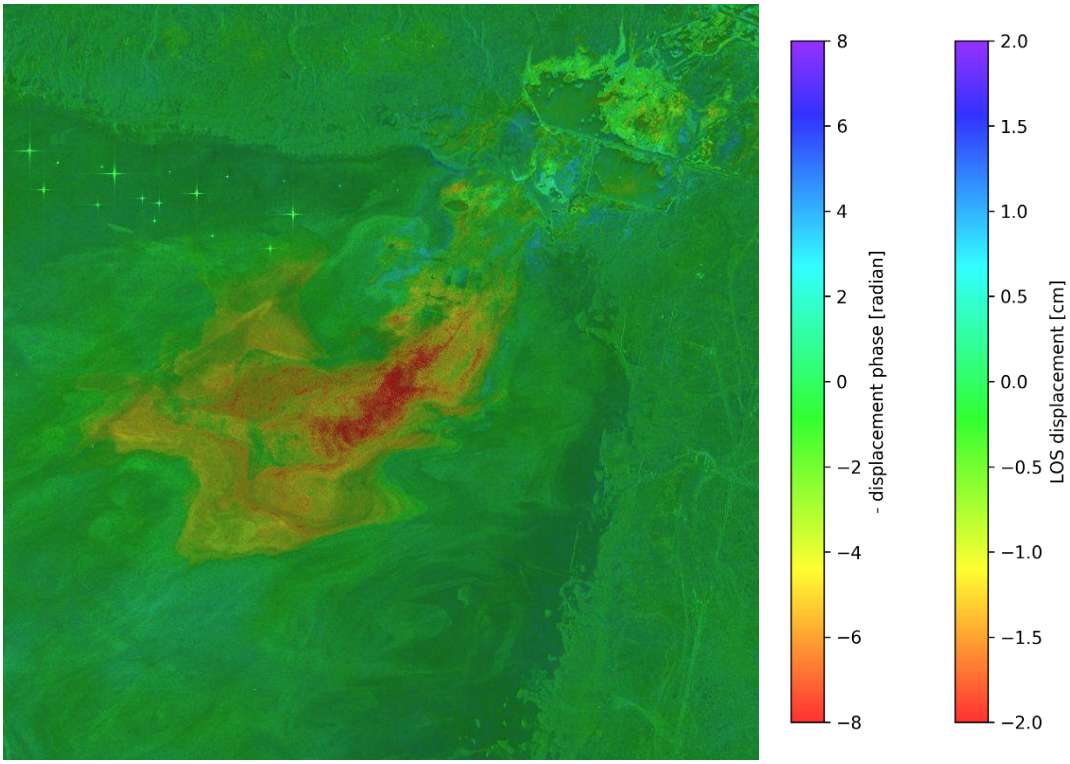


Figure 11 Line-of-sight displacement estimated using the stack of 51 ICEYE acquisitions Oversampled 1-arc-second Copernicus DEM height (left) and ICEYE based updated DEM for an 5.6km x 5.6 km area (section 1) including parts of a salt lake area with corner reflectors. A fine cyclic color scale was used to make difference between the two height maps better visible. Negative LOS displacements correspond to a displacement away from the satellite.

In this area we also observed significant displacement phase over a part of the salt lake. Figure 11 shows the displacement and displacement phase between the first and the last acquisition. Noticing that the size of the deformation pattern is significantly larger than the size of the spatial filter used in the atmospheric path delay estimation we used a modified atmosphere estimation for the moving area. To avoid subtracting deformation phase the atmospheric path delay for the moving area is found by interpolation of the atmospheric path delay from the area around the moving area. If this is not done a relevant part of the deformation phase will be subtracted as “atmospheric phase”. LOS displacements up to 2cm (away from the sensor) were observed between the first and last scene.

5. ACKNOWLEDGMENT AND COPYRIGHTS

We acknowledge ICEYE to provide us the SAR data and Innosuisse for the financial support in the EUROSTARS Project E! 113220 RAMON.

.